Segmentation of Head and Neck CT Scans Using Atlas-based Level Set Method

Xing Zhang[1], Jie Tian[1], Yongfang Wu[1], Jian Zheng[1] and Kexin Deng[2]

July 20, 2009

[1]Medical Image Processing Group, Institute of Automation Chinese Academy of Sciences. E-mail: tian@ieee.org, Tel: +86-10-82628760, Fax: +86-10-62527995. P. O. Box 2728, Beijing 100190, China.
[2]Life Science Research Center, Xidian University, Xi'an, Shaanxi, 710071, China

Abstract

In this paper, we present an atlas-based level set automatic method for segmenting anatomical structures in head and neck CT data, such as mandible and brainstem. The proposed method is a hybrid method that combines two aspects. First, we register the atlas image to the image to be segmented using an intensity-based non-rigid image registration algorithm based on B-spline, the corresponding binary image of the atlas is also resampled into the reference image coordinate system according to the deformation field obtained from the registration process. Second, based on the initialization of the deformed atlas binary mask, the level set function is evolved to segment the object of interest in the test image. The proposed method was tested on CT images of head and neck and compared with expert segmentation of mandible and brainstem. The evaluation results show the method is available and effective.

Latest version available at the Insight Journal [http://hdl.handle.net/1926/1338]

Contents

1 Introduction

Head and neck cancers account for approximately 3 to 5 percent of all cancers in the United States. It is estimated that about 39,000 men and women in this country developed head and neck cancer in 2005. The primary treatments for head and neck cancer are radiotherapy, surgery and chemotherapy. As the most common form of treatment, intensity-modulated radiotherapy (IMRT) [6] is preferable for reducing incidental damage to healthy cells and structures than some conventional radiation techniques. Accurate Segmentation of anatomical structures in CT scans is a prerequisite for effective computer-aided IMRT planning. While manual delineation of objects in 3D medical images by a trained expert is tedious, time-consuming and suffers from large inter- and intra-rater variability, the challenge currently confronted by clinical application is automatic segmentation of anatomical structures in head and neck CT data.

As a consequence of the nature of image acquisition process, noise and the partial volume effect is inherent in all medical data. Furthermore, mandibles are connected with skull and brainstems are indiscernible from surrounding soft tissues in CT scans, which make automatic segmentation a difficult problem. Due to the complex geometry and inter-person similarity of the same structure in H&N CT scans, how to maximumly employ prior anatomical knowledge is critical for accurate segmentation. Since prior knowledge is often included in reference images or atlases, atlas-based segmentation [3] has become a standard approach to incorporate high-level shape priors in medical image segmentation. Atlas-based segmentation is often known as registration-based segmentation, which is widely applied in MRI brain structures segmentation. In these method, an atlas image is registered to a subject image, and then segmentation image of the atlas is mapped to the new image according to the spatial transform obtained from the registration process. Nevertheless, the transformed contour produces discontinuities and holes, which need to be eliminated or smoothed by post-process.

2 Method

The proposed atlas-based segmentation method is a hybrid method incorporating registration and segmentation process. We illustrate the method discussed in this section by segmenting mandibles and brainstems from 8 testing data of head and CT scans acquired clinically. An atlas is often generated by labeling structure of interest of an actual image and which can be also regarded as ground truth. In this paper, we refer to the 10 training datasets with expert segmentation results as the atlas images. The flow chart of the proposed method is shown in Fig. 1.

In the registration process, an atlas image is to be deformed and testing data remains fixed. Correspondingly, we use the resulting spatial transformation to map the segmentation result of the atlas to the testing image. Considering that inter-personal variability of the same structure, we prefer a B-spline deformable image registration method rather than rigid registration techniques. Especially, atlas construction and selection has a substantial impact on the segmentation accuracy. We utilize image similarity metric to choose the best atlas for an testing image. Finally, the initial deformed segmentation of an atlas produce discontinuities and holes and may not accurate for the testing data, level set evolution is employed to track the accurate boundary of structures. The three steps are described in more details below.

2.1 Non-rigid Registration based on B-spline

The B-spline non-rigid registration method employs free-form deformation (FFD) based on the B-spline function as the transformation model [1, 5]. Assuming that a 3-D image I, where I(x,y,z) represents the

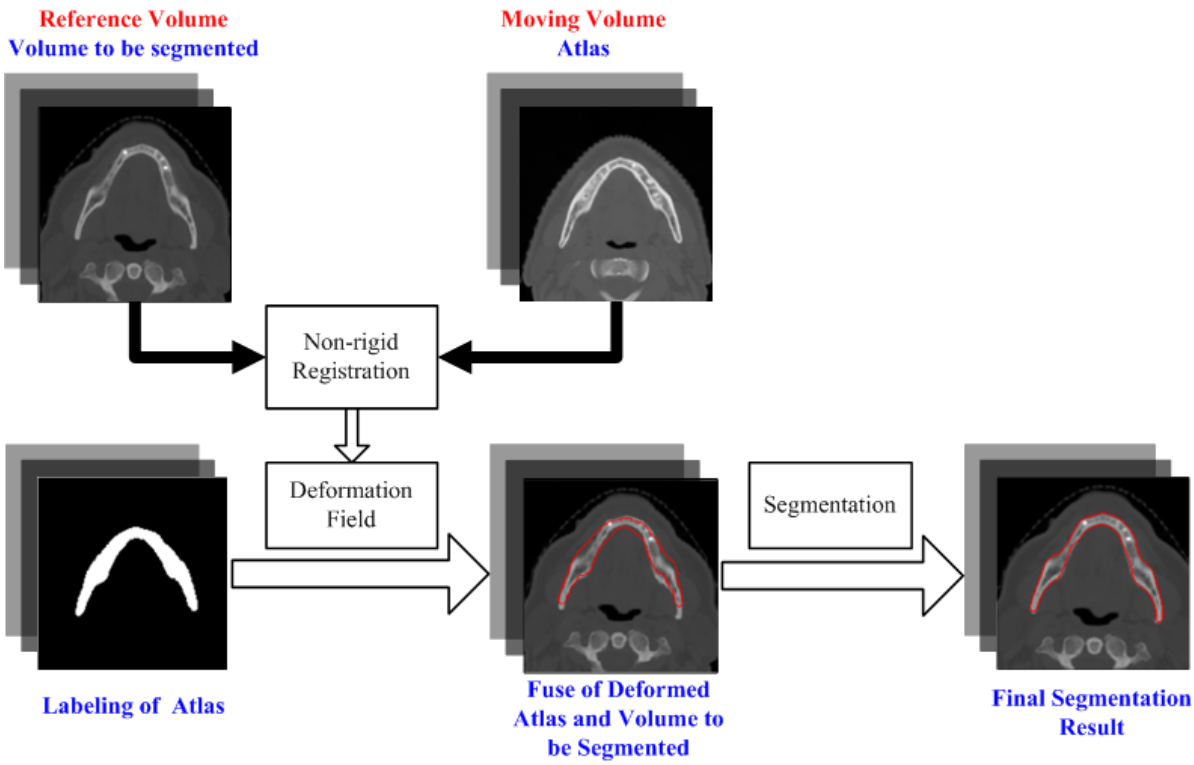

Figure 1: The flow chart of the proposed atlas-based segmentation method.

image intensity at voxel [x,y,z]. φ denotes a $n_x \times n_y \times n_z$ uniformly spaced grid of control points $\varphi_{i,j,k}$ covering the 3D reference image, the spacings between the control points in x, y and z are defined with δ_x, δ_y and δ_z respectively. The transformation T can be computed from the positions of the surrounding $4\times4\times4$ control points.

$$T(x,y,z) = \sum_{l=0}^{3}\sum_{m=0}^{3}\sum_{n=0}^{3} B_l(u)B_m(v)B_n(w)\varphi_{i+l,j+m,k+n} \tag{1}$$

where $i = \left\lfloor \frac{x}{\delta_x} \right\rfloor - 1$, $j = \left\lfloor \frac{x}{\delta_y} \right\rfloor - 1$, $k = \left\lfloor \frac{x}{\delta_z} \right\rfloor - 1$, $u = \frac{x}{\delta_x} - \left\lfloor \frac{x}{\delta_x} \right\rfloor$, $v = \frac{y}{\delta_y} - \left\lfloor \frac{y}{\delta_y} \right\rfloor$, $w = \frac{z}{\delta_z} - \left\lfloor \frac{z}{\delta_z} \right\rfloor$. $B_l(u)$, $B_m(v)$ and $B_n(w)$ are basis functions of the cubic B-spline:

$$\begin{aligned} B_0(u) &= (1-u)^3/6 \\ B_1(u) &= \left(3u^3 - 6u^2 + 4\right)/6 \\ B_2(u) &= \left(-3u^3 + 3u^2 + 3u + 1\right)/6 \\ B_3(u) &= u^3/6 \end{aligned} \tag{2}$$

A normalized mutual information (NMI) metric function was used as the auto-mapping similarity measure. It is defined as

$$S_{NMI} = \frac{H(R) + H(F)}{H(R,F)} \tag{3}$$

where $H(R)$ and $H(F)$ are entropy of the reference and transformed testing images, respectively, and $H(R,F)$ denotes their joint entropy which is computed by estimating the joint histogram of the two images. The NMI value peaks when both images are aligned and this metric is limited to images in the same modality. To find the optimal transformation, the limited memory, quasi-Newton algorithm for bound constrained optimization (L-BFGS-B) was employed to minimize the estimated NMI function.

2.2 Atlas Selection

Atlas selection has a substantial impact on the segmentation accuracy. Four different approaches for atlas image selection are summarized and evaluated in [4, 3]: segmentation with an individual atlas (IND), segmentation with an average-shape atlas (AVG), segmentation with the most similar atlas for an image (SIM) and simultaneous segmentation with multi-atlases (MUL). The IND strategy is picking the atlas subjectively according to the best quality and least artifacts. The IND strategy construct an average-shape atlas or probabilistic atlas from a series of individual atlas. However, inter-personal averaging cause lost of detailed shape information. The MUL scheme which relates to fuse multiple segmentation results using multi-atlases is more robust but notable runtime consumption as the numbers of atlases increases.

The SIM strategy was applied in the proposed method. We registered a testing dataset to the 10 atlas and the atlas with the highest NMI value after non-rigid registration was selected for segmentation.

2.3 Level Set Tracking

Though the atlas binary mask of the structure is mapped to the testing data, the deformed contour produce discontinuities and holes and may not accurate for the testing data. A level set method without re-initialization [2] was employed to smooth and track the the accurate boundary of the structure. The level set function consists of three terms: an internal energy term penalizing the deviation from a signed distance function (SDF), an weighted curve length external energy and an weighted region area external energy.

$$\varepsilon(\phi) = \int_{\Omega} \frac{1}{2}(|\nabla\phi| - 1)^2 \, dxdydz + \lambda \int_{\Omega} g\delta(\phi)|\nabla\phi| \, dxdydz + \nu \int_{\Omega} g\mathrm{H}(-\phi)dxdydz \tag{4}$$

where ϕ denotes the level set function, g is the edge indicator function that decreases with gradient. $H(\bullet)$ and $\delta(\bullet)$ are the Heaviside and Dirac function, respectively.

We covered the deformed binary atlas mask on the testing data. The above level set function can be initialized with positive and negative constant outside and inside the contour obtained from the binary mask, respectively. This energy model enables large time step and therefore is more computationally more efficient than the geometric active contours (GAC). Comparison of the initial deformed contour and the final level set evolution contour is shown in Fig. 2.

3 Experiments and Results

Before the registration and segmentation process, we select a $150 \times 140 \times 50$ and $70 \times 50 \times 50$ (unit: pixels) bounding box for mandible and brainstem respectively in each volume. The control point grid size in cubic B-spline registration is $5 \times 5 \times 5$ and other parameters in level set tracking process are set with $\lambda = 3.0$, $\nu = 2.0$ and $\tau = 0.0175$ for mandibles and $\lambda = 1.0$, $\nu = 0.8$ and $\tau = 0.0175$ for brainstems.

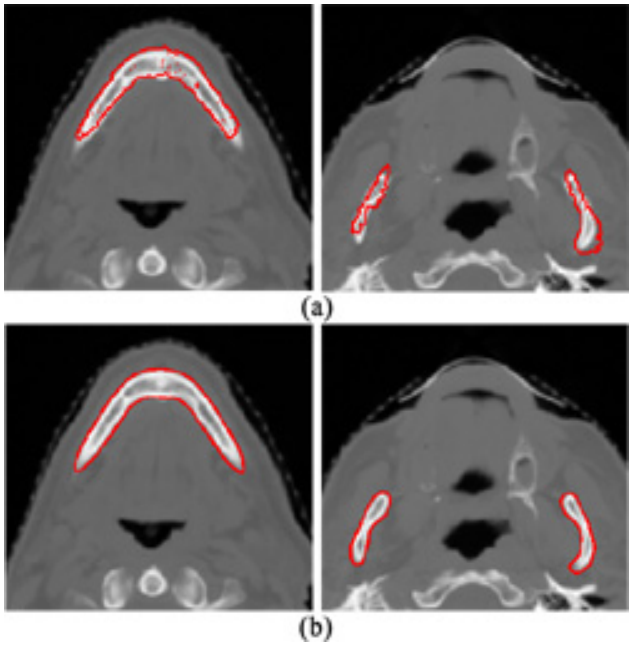

Figure 2: Comparison of our segmentation results (red contour) and the ground truth (green contour). (a) Initial contour obtained from the deformed atlas binary mask; (b) Final contour after level set evolution.

Dataset No.	Mean HD	Median HD	No. of slices (HD > 3 mm)
11	5.57	2.76	39 (17)
12	12.13	3.30	40 (23)
13	5.70	2.93	35 (16)
14	12.82	3.77	34 (24)
15	12.25	2.64	37 (14)
16	7.49	3.09	35 (18)
17	8.67	3.09	43 (23)
18	4.98	2.11	37 (13)

Table 1: Hausdorff distance (HD) statistics for mandible segmentation in the testing datasets.

The evaluation compare our results with ground truth of the expert manual segmentation. A screenshot of the comparison is shown in Fig. 3. The Hausdorff distance and volumetric overlap (Dice metric) are used as criteria in axial slice for quantitative comparison. Table. 1, 2, 3, 4 summarize the evaluation results according to the two main criteria.

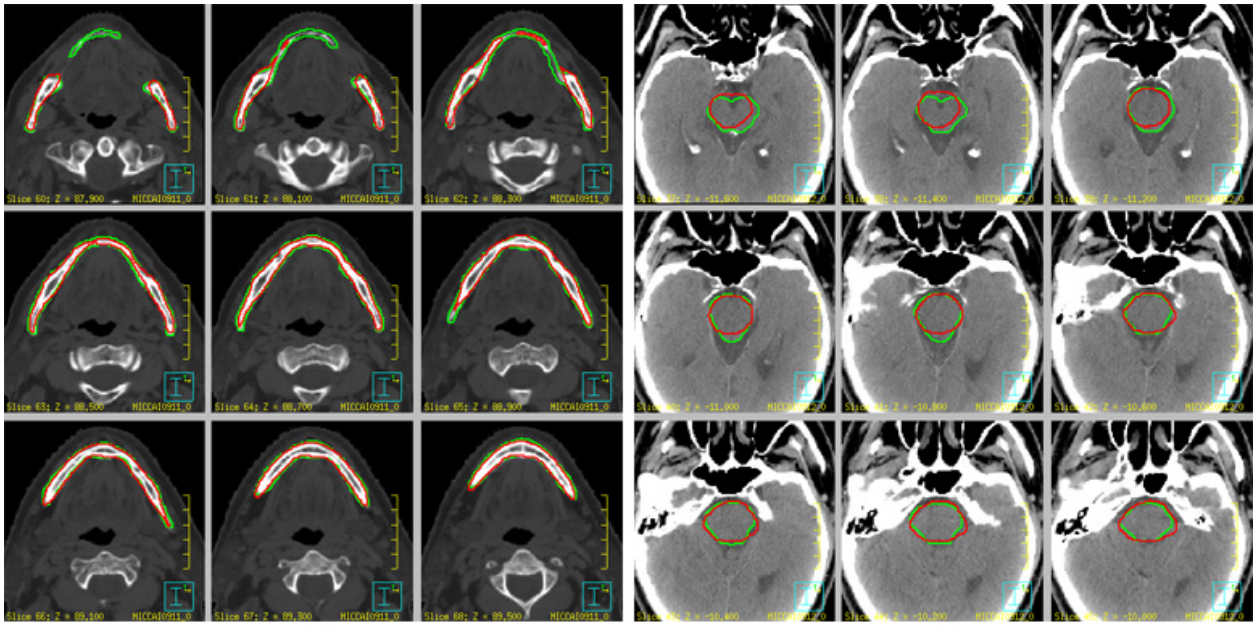

(a) (b)

Figure 3: Comparison of our segmentation results (red contour) and the ground truth (green contour). (a) Comparison of mandible segmentation result for the testing dataset MICCAI09-12; (b) Comparison of brainstem segmentation result for the testing dataset MICCAI09-12

Dataset No.	Average slice OV	Median slice OV	Total volume OV
11	83.2 %	86.7 %	85.5 %
12	80.6 %	85.4 %	86.3 %
13	85.3 %	86.3 %	88.2 %
14	74.7 %	79.1 %	85.4 %
15	86.0 %	91.1 %	89.5 %
16	80.6 %	85.6 %	88.2 %
17	86.0 %	89.7 %	89.1 %
18	86.7 %	91.5 %	91.2 %

Table 2: Overlap (OV) statistics for mandible segmentation in testing datasets.

4 Discussion and Conclusions

In the MICCAI Head and Neck Auto-Segmentation Challenge 2009, we employed the atlas-based segmentation method to segment mandibles and brainstems in head and neck CT scans. The proposed method can maximumly incorporate shape prior of the structure and the evaluation results of the testing data demonstrate the availability and effectiveness of the method. In future work, we will use the method to segment other structures including bone and soft tissue structure to testify validity of the method. Nevertheless, the most similar atlas selection strategy need improved since registration to each atlas image is a time-consuming

Dataset No.	Mean HD	Median HD	No. of slices (HD > 3 mm)
11	5.48	5.39	28 (28)
12	4.79	4.88	29 (28)
13	-	-	-
14	6.99	5.61	30 (29)
15	-	-	-
16	4.40	3.97	27 (25)
17	4.92	4.14	27 (24)
18	5.24	4.72	29 (26)

Table 3: Hausdorff distance (HD) statistics for brainstem segmentation in the testing datasets.

Dataset No.	Average slice OV	Median slice OV	Total volume OV
11	77.9 %	81.4 %	81.7 %
12	84.5 %	84.5 %	86.4 %
13	-	-	-
14	74.6 %	79.5 %	76.9 %
15	-	-	-
16	81.1 %	80.9 %	83.6 %
17	82.5 %	81.9 %	84.1 %
18	79.8 %	80.4 %	80.9 %

Table 4: Overlap (OV) statistics for brainstem segmentation in testing datasets.

work. A probabilistic atlas can be taken into consideration to solve the problem.

5 Acknowledgements

This work is supported by NBRPC (2006CB705700), PCSIRT (IRT0645), CAS SREDP (YZ0642, YZ200766), JRFOCYS (30528027), NSFC (30672690, 30600151, 60532050, 60621001, 30873462), BNSF (4071003), TKPBEC (KZ200910005005) in China.

References

[1] Seungyong Lee, George Wolberg, Kyung-Yong Chwa, and Sung Yong Shin. Image metamorphosis with scattered feature constraints. *IEEE Transactions on Visualization and Computer Graphics*, 2(4):337–354, 1996. 2.1

[2] Chunming Li, Chenyang Xu, Changfeng Gui, and Martin D. Fox. Level set evolution without re-initialization: A new variational formulation. In *Proceedings of the 2005 IEEE Computer Society Conference on Computer Vision and Pattern Recognition (CVPR'05)*, pages 430–436, 2005. 2.3

[3] T. Rohlfing, R. Brandt, R. Menzel, D. Russakoff, and Jr. Maurer. *Quo Vadis, Atlas-Based Segmentation?*, pages 435–486. Kluwer Academic Publishers, 2005. 1, 2.2

[4] Torsten Rohlfing, Robert Brandt, Randolf Menzel, and Calvin R. Maurer Jr. Evaluation of atlas selection strategies for atlas-based image segmentation with application to confocal microscopy images of bee brains. *NeuroImage*, 21(4):1428–1442, 2004. 2.2

[5] D. Rueckert, L. I. Sonoda, C. Hayes, D. L. G. Hill, M. O. Leach, and D. J. Hawkes. Nonrigid registration using free-form deformations: Application to breast mr images. *IEEE Transactions on Medical Imaging*, 18(8):712–721, 1999. 2.1

[6] Han X, Hoogeman MS, Levendag PC, Hibbard LS, Teguh DN, Voet P, Cowen AC, and Wolf TK. Atlas-based auto-segmentation of head and neck ct images. In *International Conference on Medical Image Computing and Computer-Assisted Intervention (MICCAI'08)*, pages 434–441, 2008. 1